Final Report: Year 2 (Reporting Year: 2018-2020), FK # 129664

Background

Advances in the molecular profiling of non-small cell lung cancer (NSCLC) have helped the discovery of alterations in genetic drivers that have paved the way for the development of targeted therapies. These advances have changed the therapeutic landscape of NSCLC and improved clinical outcomes. The majority of distinct genetic alterations occur in lung adenocarcinoma, the most common histology of NSCLC. (Cancer Genome Atlas, Nature 2014;511:543-50., Grosse et al. Diagn Pathol. 2019 Feb 11;14(1):18., Rosell R et al. Lancet Oncol 2012;13:239-46.) The EGFR/RAS/BRAF/MEK/ERK pathway transduces mitogen signals from the cell membrane to the nucleus, a critical pathway in the progression of many human cancers, including NSCLC. The V-raf murine sarcoma viral oncogene homolog B (BRAF) gene encodes RAF serine/threonine kinase proteins, including ARAF, BRAF, and CRAF isoforms. The mutations or overexpression of BRAF constitutively results in an increase in oncogenic signaling through MEK, and the activation of the mitogen-activated protein kinase (MAPK) pathway promotes cell growth, proliferation, and survival. However, the clinical relevance of BRAF genetic alterations in NSCLC is not fully understood. Here we aimed to analyze a cohort of patients to study BRAF genetic alterations' role and identify potential novel targets in NSCLC. (Planchard D et al. Lancet Oncol 2016;17:984-93.)

Materials and methods

Tissue processing

We included early-stage NSCLC patients' primary tumors; samples were obtained by lung biopsy or resection. Tumors were fixed and processed into paraffin blocks. Tissue microarray (TMA) construction from FFPE blocks was performed as previously described. (Battifora H (1986) Methods in laboratory investigation) We prepared 4-micron sections from each tissue block and transferred the tissue on charged glass slides using a microtome. Slides were stained for H&E. A pathologist reviewed and marked the tumor area for punch tissue subtraction. Two 5-mm punches of tissue were taken from each primary tumor tissue block for the TMA.

RNAscope

RNAScope® *in situ* hybridization assay was performed on TMAs from human adenocarcinomas using RNAScope® Multiplex Fluorescent Kit v2 according to the manufacturer's instructions (Advanced Cell Diagnostics Pharma Assay Services, Newark, CA, USA). Briefly, 4 μm formalin-fixed paraffin-embedded TMA sections were pretreated with antigen-retrieval buffer, heat, and protease before hybridization with the following target oligo probes: 3plex-Hs-Positive Control Probe (ACDBio, cat: 320861), 3plex-Hs-Negative Control Probe (ACDBio, cat: 320871), Hs-BRAF-C1 (ACDBio, cat: 595251). Preamplifier, amplifier, and AMP-labeled oligo probes were then hybridized sequentially, followed by chromogenic precipitate development. Cy3 (red) fluorochrome was used to visualize binding spots for amplified probes. Each sample was quality controlled for RNA integrity with a positive control probe specific to the housekeeping genes with a negative control probe. We optimized the

pretreatment conditions to establish the maximum signal-to-noise ratio. We identified specific RNA staining signals as red punctate dots, and nuclei stained with 4′,6-diamidino-2-phenylindole (DAPI) appeared light purple. Imaging was performed with Zeiss LSM 780 Confocal microscope. To perform RNAScope® - IHC codetection, an anti-E-cadherin monoclonal antibody (cat:) was used to identify tumor cells of epithelial origin. The primary antibody was applied overnight before the hybridization steps. Antigen-antibody complexes were crosslinked by neutral buffered formalin for 30 minutes before protease treatment. Slides were incubated with ALEXA A488 (green) anti-mouse secondary antibody for 45 minutes after signal amplification and detection of RNAScope® probes.

Scoring with QPath Software

After selecting representative regions on slides containing no positive RNAscope® staining, we measured the total intensity of the selected background regions and calculated average background intensity (Average Intensity of Background per Pixel) using the following equation:

Average Background Intensity = ∑ integrated intensity of selected background regions / ∑ area of selected background regions

To quantify average intensity per single dot, first, we selected at least 20 single signal dots for every visual field and measured each dot's area and total Intensity. Then, we used the area of each dot to screen whether the dot is a true single dot and calculated the average intensities for every single dot:

Average Intensity per Single Dot = ∑ integrated intensity of selected dots - average background intensity × ∑ area of selected dots/number of selected dots

To measure the total area of the region of interest (ROI) and total intensity of ROI, we used average intensity per single dot. We calculated the total dot number in the ROI:

Total Dot Number in ROI = total intensity of ROI - average background intensity × total area / average intensity per single dot

Next, we counted the number of cells in the ROI by counting DAPI positive nuclei and used this value to calculate the average dot number per cell.

Average dot number per cell = total dot number in ROI / total number of cells in ROI

We used the DAPI nuclear staining to define each cell region by assigning the cell's radius and assigning each cell as one ROI. Then, we counted the dot number in each ROI as previously described. We calculated an integrated expression score (0-3) for all tumor cores based on dots' average density and raw intensity data. We included all cores per patient in TMAs, so an average BRAF expression score was derived from the values of each core for every patient.

Immunohistochemistry (IHC)

To analyze the potential associations of immune checkpoint inhibition therapy, we performed the programmed death protein 1 (PD-1) and PD-1 ligand (PD-L1) IHC. We used 4 μm sections cut from every FFPE TMA block for IHC staining. Staining was performed on a Leica Bond RX autostainer using rabbit monoclonal antibody for PD-L1 diluted 1:300 (CST, cat: 13684S) and rabbit monoclonal antibody for PD-1 diluted 1:400 (CST, cat: 86163). Slides were stained using the Bond Polymer Refine Detection kit (#DS9800) with Leica IHC Protocol F, and exposed to epitope retrieval 1 (low pH) for twenty minutes. Clearing and dehydration of slides were performed on an automated Tissue-Tek Prisma platform and then coverslipped using a Tissue-Tek Film coverslipper. For tumor-cell-PD-L1 expression, scoring was based on staining intensity multiplied by the number of expressing cells per TMA core. The number of expressing cells was calculated for each TMA core to assess immune cell- and macrophage- PD-L1 and immune cell PD-1 expression. We averaged the calculated values of the cores for every patient. Scores were normalized to a 6-level scale (0-5) based on the k-means clustering method. Cancer cells, immune cells, and macrophages were identified by routine HE staining. Staining protocols were optimized on healthy human lung and tonsil tissues.
We also used 4 μm fresh-cut TMA sections for developing new targets, including staining oncofetal chondroitin sulfate (OCS) expression. OSC IHC was performed using the Ventana Discovery platform, as described previously (Salanti, A et al. Cancer Cell 2015, 28, 500–514.). We analyzed the intensity and percent positivity for both pericellular and extracellular immunostaining as described earlier (Oo, H.Z.; Lohinai, Z.; Cancers 2021, 13, 4489). While an overall score was calculated for each tissue core, an average score of 100 to 300 was considered as OCS high. We correlated high vs. low OCS expression of both tumor and stromal cells, according to EGFR and KRAS mutations, clinicopathological characteristics including disease-free survival (DFS), and overall survival (OS).

Statistical analyses

We used the Mann–Whitney U-test to compare BRAF, OSC, and PD-L1 expression between patient groups according to clinicopathological characteristics. P-values < 0.05 indicate the significance, and all p-values were two-sided. We performed survival analysis with Kaplan-Meier curves and a comparison of survival curves with the log-rank test. Statistical analyses were performed using the PASW Statistics 22.0 package (SPSS Inc., Chicago, IL, USA).

Progress and Results of Research (Year 1-2)

Advanced non-small-cell lung cancer (NSCLC) with BRAF mutations are present in approximately 2-3% of cases (Leonetti A et al. Canc Treat Rev 2018;66:82e94, Wiesweg M et al. Eur J Cancer. 2021 May;149:211-221.).
Our preliminary study showed only a few cases with BRAF mutations using Sanger sequencing; therefore, we could not perform statistical analysis or draw firm conclusions as expected in the original research plan. This is in line with others who recently showed that out of 2211 NSCLC cases in a retrospective analysis, only 3.26% of patients with BRAF-mutated

NSCLC with less than 2% non-V600E mutations were identified. (Wiesweg M et al. Eur J Cancer. 2021 May;149:211-221.)
Accordingly, we decided to focus on BRAF RNA expression expected to involve a number of patients that can be applied in further statistical analyses. Notably, RNAscope is a novel in situ hybridization (ISH) assay that we primarily used to discover target RNA within tumor cells. The assay used represents a significant advancement in target-specific signal detection.
To our knowledge, the RNA expression patterns of the wild-type (WT) BRAF proteins have not been investigated in NSCLC and might result in enhanced downstream signalization. Moreover, the transcriptomic analysis of BRAF can reveal new insights into biology, including analysis of clinical outcomes and clinicopathological parameters. Therefore, we analyzed in situ expression of BRAF RNA by RNAscope. Then, we correlated BRAF expression scores with clinicopathological parameters, including sex, age, PD-L1 expression, pathological tumor characteristics (peritumoral infiltration, tumor necrosis, and vascular involvement), chronic obstructive pulmonary disease (COPD), diabetes, and overall survival.
We constructed a TMA and a clinical database on NSCLC that enabled us to study biomarkers, new targets, and the tumors' microenvironments, an emerging field of tumor progression.
Since immune checkpoint inhibition (ICI) was reported to significantly advanced outcomes, we stained PD-L1, a key biomarker in NSCLC, to analyze potential (ICI) therapy associations.

Tumor changes such as cell surface glycosylation regulate several pathophysiological processes, including signalization, cell-matrix interaction, angiogenesis, immune modulation, invasion, and metastasis. (Pinho, S.S et al. Nat. Rev. Cancer 2015, 15, 540–555.) Changes in glycosylation patterns are associated with carcinogenesis. (Ladenson R.P. et al. Am. J. Med. Sci. 1949;217:194–197.; Hakomori S.I. et al. Proc. Natl. Acad. Sci. USA. 1968;59:254–261.) Specifically, chondroitin sulfate (CS) alterations have been described in most solid tumors .(Khazamipour, Net al. 2020, 9, 818.) Modification of proteins with CS forms biologically active molecules called chondroitin sulfate proteoglycans (CSPG). (Ajit Varki et al., Essentials of Glycobiology 3rd ed.; N.Y., USA, 2015–2017.) Many solid tumors express placental-type CS as a secondary oncofetal (OCS) modification on proteoglycans. We hypothesized that using our TMA provides an opportunity to study broad-spectrum OCS glycosaminoglycan modification expressed on cell surface proteoglycans previously described in other solid tumors. Proteoglycans modified with distinct OCS chains can be detected and targeted with recombinant VAR2CSA (rVAR2) proteins and rVAR2-derived therapeutics.
OCS expression in lung cancer has not yet been investigated. Therefore, our further aim was to analyze the microenvironment, including immune cells, and the presence of PD-L1 and OCS expression in NSCLC.

In the first part of our study, tumor samples of 64 resected adenocarcinoma patients were stained using RNAscope, and the average BRAF expression score was calculated for every patient. There were no patients with a score below 1, meaning that BRAF is expressed at a minimum baseline levels in adenocarcinomas. Our cohort's average BRAF expression score was 2.17 ± 0.46, with an overall low level of intratumoral heterogeneity, where expression scores for different TMA cores showed a strong positive correlation between each other

(average, r = 0.62, p<0.001). BRAF RNA was predominantly expressed in tumor nests, inside E-cadherin-positive cancer cells (**Fig 1A and B**), only with scattered expression in the stroma.

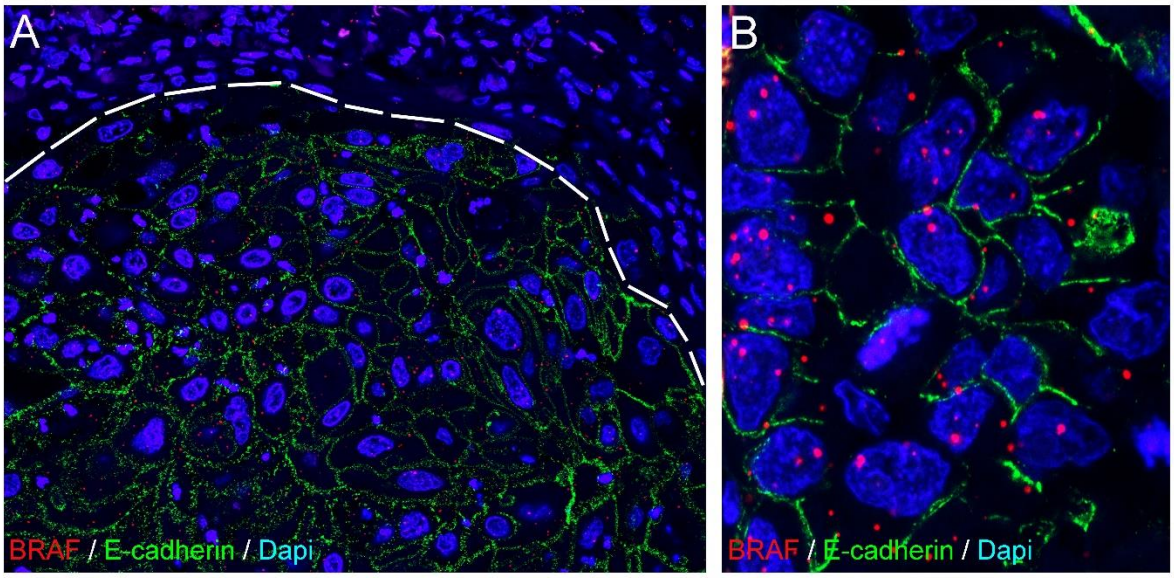

Figure 1. BRAF RNA expression in adenocarcinomas. BRAF RNA was predominantlyessed in E-cadherin positive epithelial tumor nests (A, inside dashed lines, B) and scattered stromal cells.

Next, we stratified patients according to various clinicopathological characteristics and evaluated average BRAF expression scores in patient groups. There was no significant difference according to sex (2.12 ± 0.49 vs 2.2 ± 0.41, p=0.404, **Fig 2A**), presence of COPD (2.12 ± 0.48 vs 2.3 ± 0.31, p=0.179, **Fig 2B**) or diabetes (2.14 ± 0.47 vs 2.41 ± 0.34, p=0.178, **Fig 2C**) regarding BRAF expression. Smoking however, showed a weak significant negative correlation with BRAF expression (r = -0.29, p=0.043) and never smokers express significantly higher levels of BRAF RNA compared to current smokers (2.77 ± 0.09 vs 2.02 ± 0.55, p=0.039, **Fig 2D**).

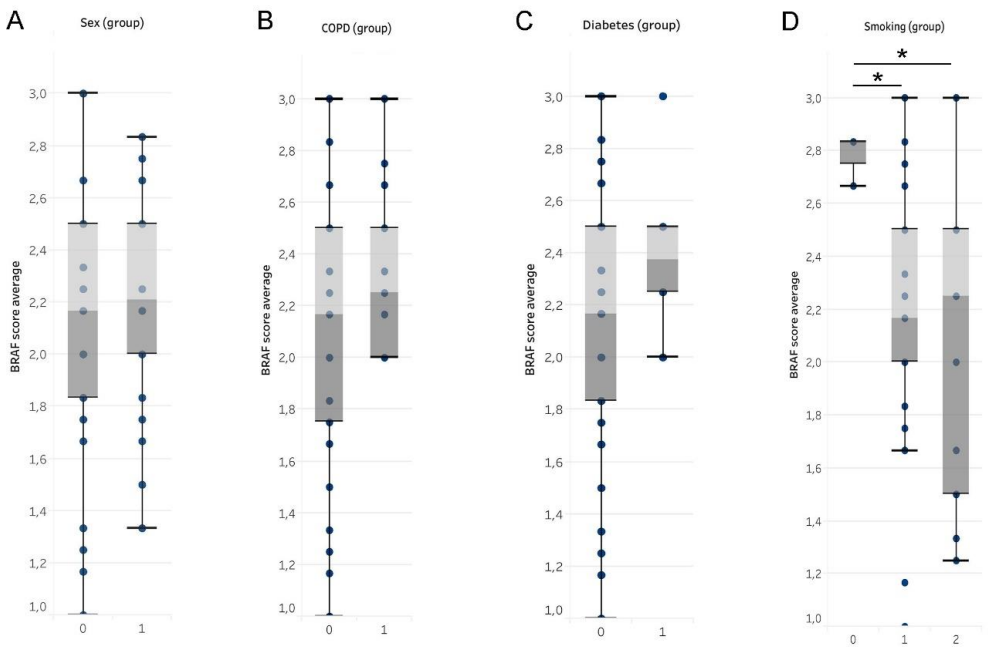

Figure 2. BRAF expression according to clinicopathological parameters, including Sex (A), COPD (B), Diabetes (C), and Smoking (D). Metric data were shown as mean and corresponding SEM, and graphs indicate the mean and corresponding 95% CI. Statistical significance *$P < 0.05$; **$P < 0.01$.
Sex: 0=male 1=male. COPD and diabetes: 0=condition not present, 1=condition present. Smoking: 0=never smoker, 1=ex-smoker, 2=current smoker

To reveal BRAF expression according to the PD-L1 phenotype, we compared high PD-L1 expressor (aggregate score: 3-4-5) patients with low expressors (aggregate score: 0-1-2). PD-L1 expression was assessed in tumor cells, macrophages, and non-macrophage immune cells, whereas PD-1 expression was assessed in immune cells. There was no significant difference in BRAF RNA expression between tumor PD-L1-high vs low patients (2.34 ± 0.43 vs 2.17 ± 0.6, p=0.399, **Fig 3A**), and between immune cell PD-L1-high vs low patients (1.79 ± 0.39 vs 2.19 ± 0.45, p=0.089, **Fig 3B**). In contrast, BRAF expression showed significant difference between macrophage PD-L1-high vs low patients (1.93 ± 0.34 vs 2.25 ± 0.43, p=0.047, **Fig 3C**). According to Spearman's correlation, this was supported by the fact that macrophage PD-L1 expression shows a moderate negative correlation with BRAF expression (r = -0.35, p=0.028). PD-1 expression in immune cells showed no significant association with BRAF RNA level in tumors (2.16 ± 0.38 vs. 2.17 ± 0.52, p=0.912, **Fig 3D**).

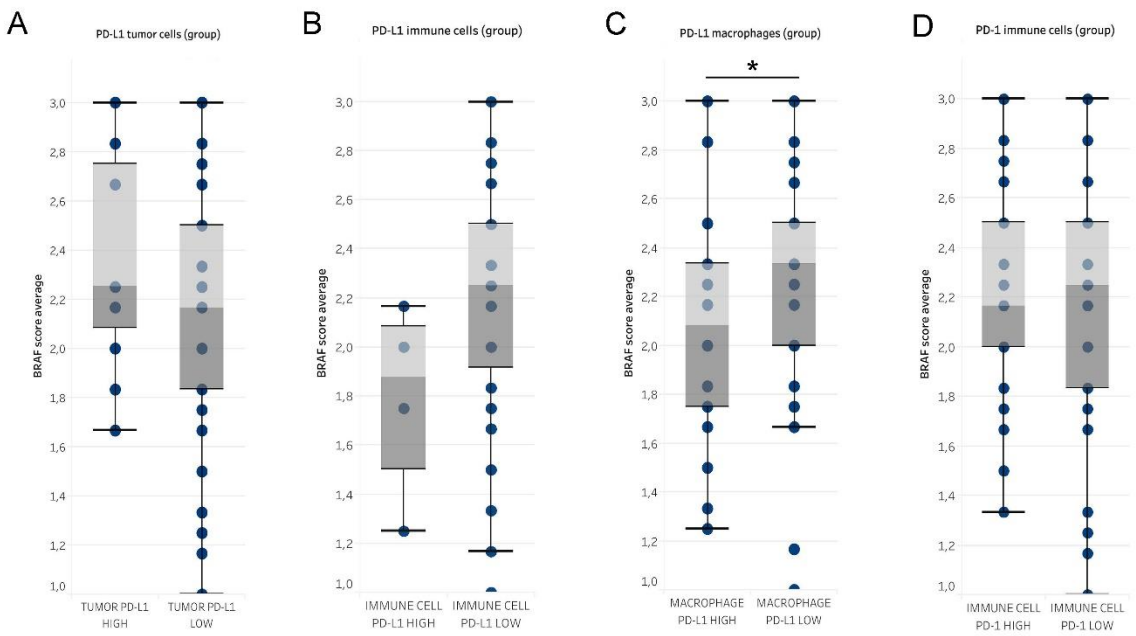

Figure 3. BRAF expression according to PD-L1 expression in tumor cells (A), immune cells (B), macrophages (C), and PD-1 expression in immune cells (D). Metric data was shown as mean and corresponding SEM, and graphs indicate the mean and corresponding 95% CI. Statistical significance $*P < 0.05$; $**P < 0.01$.

Among pathological characteristics of tumors, tumor necrosis showed a moderate positive correlation with BRAF expression (r = 0.33, p=0.008), and patients with tumor necrosis detected express significantly higher levels of BRAF RNA (1.87 ± 0.46 vs. 2.24 ± 0.43, p=0.007, **Fig 4A**). Tumors with vascular involvement exhibited no significant difference in BRAF expression compared to tumors with no vascular involvement (2.14 ± 0.44 vs. 2.23 ± 0.49, p=0.438, **Fig 4B**).

To reveal the association of clinical outcome with WT BRAF expression, we performed survival analysis stratifying patients to BRAF-high and BRAF-low expressors using expression score 2 as cut off (BRAF-high > 2 > BRAF-low). Patients with low BRAF expression score (2 >) showed significantly increased OS, compared to high BRAF-expressors (2 <) (58 vs. 27 months, [HR]: 0.465, p=0.0001, **Fig 5A**), this was supported by correlation analysis according to Spearman, that showed a significant negative correlation between BRAF expression and OS (r = -0.45, p<0.001). **Fig 5B** shows diverging KM curves for OS, according to stratification of BRAF expression.

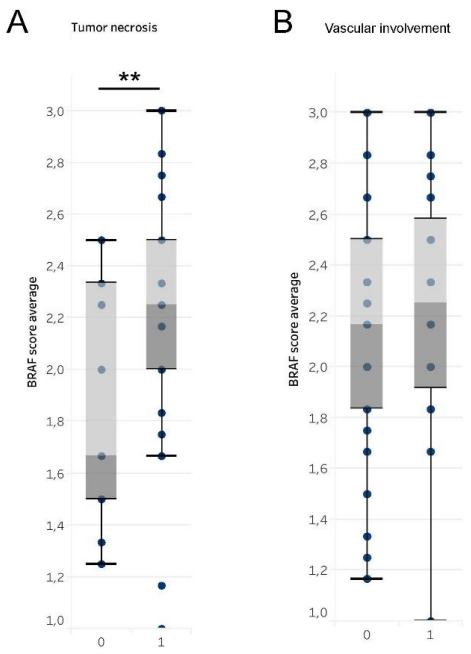

Figure 4. BRAF expression according to tumor pathology, including the presence of tumor necrosis (A), or peritumoral infiltration. Metric data were shown as mean and corresponding SEM, and graphs indicate the mean and corresponding 95% CI. Statistical significance *$P < 0.05$; **$P < 0.01$

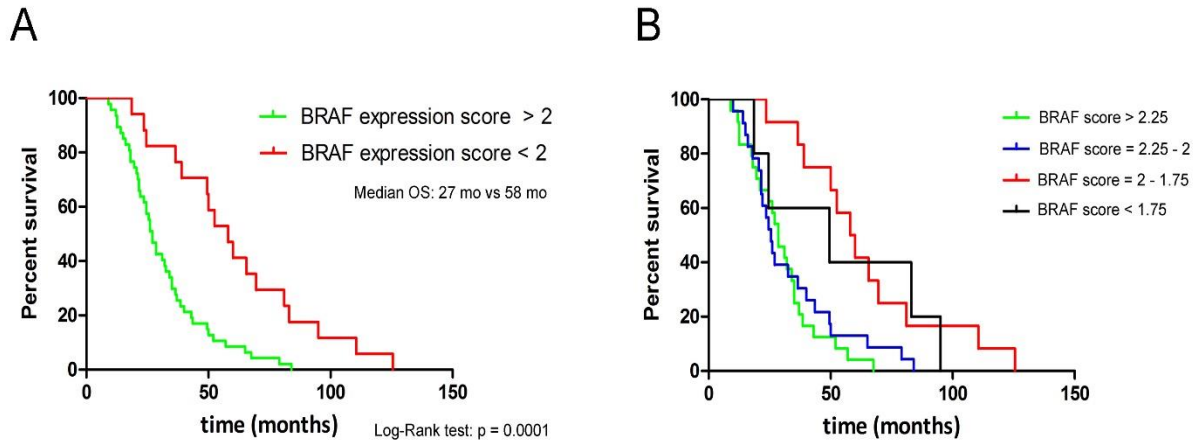

Figure 5. Survival according to BRAF expression. KM curves show survival in patients with high- (>2) versus low (<2) BRAF expression (A). Survival in different patient groups stratified according to BRAF expression score (B).

For the OCS analysis, we stained using IHC a total of 493 patients diagnosed with NSCLC in international collaboration as described by our group in a recent publication. (Oo HZ, Lohinai Z et al. Oncofetal Chondroitin Sulfate Is a Highly Expressed Therapeutic Target in Non-Small Cell Lung Cancer. Cancers (Basel). 2021 Sep 6;13(17):4489.)
The mean age at diagnosis was 65.6 ± 9.8 years. The median overall survival (OS) of the cohort was 66.7 ± 4.8 years.

There were 351 patients (71%) with low and 142 patients (29%) with high oncofetal CS expression. High oncofetal CS levels were associated with shorter DFS in all cases (39 vs. 67 months, $p < 0.01$) and smokers ($p < 0.05$) and with shorter OS for all cases (51 vs. 69 months, $p = 0.044$) and smokers ($p = 0.028$).

CONCLUSION

Our tissue microarray (TMA) provided a unique opportunity to study new targets, including BRAF and tumor microenvironments in NSCLC. BRAF RNA was widely expressed in tumor nests, inside E-cadherin-positive cancer cells only with scattered expression in the stoma. Tumor necrosis was associated with significantly higher levels of BRAF expression.
Never smokers express significantly higher levels of BRAF RNA expression compared to current smokers. Additionally, BRAF RNA expression showed a significant difference between macrophage PD-L1-high vs. low patients. The TMA set provided an opportunity to stain OCS using IHC that was extensively expressed in NSCLC. OCS is an independent prognosticator in NSCLC and a potential actionable therapeutic target.

Future directions

With the help of this grant, we are making data openly accessible, and articles are published in a format that allows data to be reused by other scientists.
We plan to continue research into the tumor microenvironment and analyze the novel targets' therapeutic relevance.

Activities Related to this Grant

In the past 24-month period of the Research Project, we presented data on our research at the World Conference on Lung Cancer. Also, we participated in several scholarly discussions with leading scientists involved in lung cancer research, diagnosis, and therapy. Results of the current project have made significant progress with published a paper and others in the process of manuscript drafting targeting submission for publication later this year. As requested by NKFIH, we state in each one that we are a recipient of an OTKA grant. With the help of the current NKFIH OTKA grant, we had the opportunity to use high-quality research methods and cooperate/network with participating clinicians and researchers with a wide range of scientific backgrounds. Balazs Santa and Csilla Kugler medical student participants awarded price at the Students' Scientific Conference, Semmelweis University, and National Students' Scientific Conference (OTDK 2019). The achieved results of the current project provide the opportunity to continue research in the field.